ЖЭТФ, 2010, том 137, вып. 6, стр. 1133–1138

ARPES SPECTRAL FUNCTIONS AND FERMI SURFACE FOR $La_{1.86}Sr_{0.14}CuO_4$ COMPARED WITH LDA+DMFT+Σ_k CALCULATIONS

I. A. Nekrasov[a]*, *E. E. Kokorina*[a], *E. Z. Kuchinskii*[a], *M. V. Sadovskii*[a], *S. Kasai*[b], *A. Sekiyama*[b], *S. Suga*[b]

[a] *Institute for Electrophysics, Russian Academy of Sciences 620016, Ekaterinburg, Russia*

[b] *Graduate School of Engineering Science, Osaka University, Toyonaka 560-8531, Osaka, Japan*

Received November 6, 2009

The slightly underdoped high-temperature system $La_{1.86}Sr_{0.14}CuO_4$ (LSCO) is studied by means of high-energy high-resolution angular resolved photoemission spectroscopy (ARPES) and the combined LDA+DMFT+Σ_k computational scheme. The corresponding one-band Hubbard model is solved via dynamical mean field theory (DMFT), and the model parameters needed are obtained from first principles in the local density approximation (LDA). An "external" **k**-dependent self-energy Σ_k describes the interaction of correlated electrons with antiferromagnetic (AFM) pseudogap fluctuations. Experimental and theoretical data clearly show the "destruction" of the LSCO Fermi surface in the vicinity of the (π,0) point and formation of "Fermi arcs" in the nodal directions. ARPES energy distribution curves as well as momentum distribution curves demonstrate a deviation of the quasiparticle band from the Fermi level around the (π,0) point. The same behavior of spectral functions follows from theoretical calculations suggesting the AFM origin of the pseudogap state.

1. INTRODUCTION

One of the puzzles of cuprate high-temperature superconductors (HTSC) that remains unsolved is the nature of the underdoped normal state, the pseudogap regime [1]. Perhaps most powerful experimental tool to access electronic properties of the pseudogap state is angular resolved photoemission spectroscopy (ARPES) [2–4]. It is commonly understood that the pseudogap state has a fluctuation origin, but the type of the fluctuations is still under discussion. Whether these are superconducting fluctuations [5] or some order parameter fluctuations (AFM(SDW), CDW, stripes, etc.) [6, 7] coexisting or competing with Cooper pairing is presently undecided.

There are several prototype compounds among high-T_c systems, e. g., the hole-doped $Bi_2Sr_2CaCu_2O_{8-\delta}$ (Bi2212) system or the electron-doped $Nd_{2-x}Ce_xCuO_4$ (NCCO) system. Extensive experimental ARPES data on Bi2212 and NCCO are available presently (see review [2]). For instance, Fermi surface (FS) maps, quasiparticle band dispersions, and even self-energy lineshapes mapped onto some models are obtained from modern ARPES measurements [6]. Into this list of prototype compounds should of course be included the first ever high-T_c hole-doped system $La_{2-x}Sr_xCuO_4$ (LSCO), which was also investigated in great detail both theoreticaly and experimentally [2].

A number of interesting physical phenomena were discovered in the normal underdoped phase (pseudogap regime). For example, the FS is partially "destroyed" in the vicinity of the so-called "hot spots" (points of crossing between the FS and the AFM umklapp surface). "Shadow bands" (partial folding of band dispersion) appear possibly as a result of a short-range AFM order. Formation of the so-called Fermi "arcs" around the Brillouin zone (BZ) diagonal, reminiscent of the parts of a noninteracting FS, is experimentally detected in numerous ARPES experiments [2]. Despite apparently the same underlying physics, the pseudogap regime demonstrates some material-specific features.

*E-mail: nekrasov@iep.uran.ru

For Bi2212, Fermi "arcs" extend almost up to the BZ border, where they are strongly blurred. NCCO also has Fermi "arcs", but the FS "destruction" looks different. The "hot spots" are well observed in NCCO, while the FS is almost restored as a noninteracting Fermi surface towards the BZ border [8].

The present paper is devoted to the pseudogap behavior in underdoped LSCO and its comparison with Bi2212 and NCCO.

According to common knowledge, high-T_c systems are usually doped Mott insulators, effectively described by the Hubbard model. The most common method to solve the Hubbard model is presently the dynamical mean field theory (DMFT) [9]. Its exactness in the infinite spatial dimension limit makes it a local approach. It is well established that high-T_c compounds have a quasi-two-dimensional nature, and therefore spatial fluctuations play an important role for their physics. To overcome this difficulty, we introduced the DMFT+$\Sigma_{\mathbf{k}}$ computational scheme [10–12] that supplies the conventional DMFT with an "external" $\mathbf{k}$-dependent self-energy. The main assumption of the DMFT+$\Sigma_{\mathbf{k}}$ scheme is the additive form of the self-energy, which allows keeping the conventional DMFT self-consistent set of equations. The DMFT+$\Sigma_{\mathbf{k}}$ approach was used to address the pseudogap problem [11], the electron–phonon coupling in strongly correlated systems [13], and a disorder-induced metal–insulator transition in the Hubbard–Anderson model [14]. For the pseudogap state, this self-energy $\Sigma_{\mathbf{k}}$ describes the interaction of correlated electrons with nonlocal (quasi)static short-range collective Heisenberg-like antiferromagnetic (AFM or SDW-like) spin fluctuations [15]. The DMFT+$\Sigma_{\mathbf{k}}$ approximation was also shown to be appropriate to describe two-particle properties, e. g., optical conductivity [16].

As a possible way of theoretical simulation of the pseudogap regime for real materials, we proposed the LDA+DMFT+$\Sigma_{\mathbf{k}}$ hybrid method [7]. It combines first-principle one-electron density functional theory calculations in the local density approximation (DFT/LDA) [17] with DMFT+$\Sigma_{\mathbf{k}}$ [18].

The LDA+DMFT+$\Sigma_{\mathbf{k}}$ method allowed us to obtain Fermi arcs and the "hot spot" behavior for both electron-doped (e. g., $Nd_{1.85}Ce_{0.15}CuO_4$ (NCCO) [8] and $Pr_{1.85}Ce_{0.15}CuO_4$ (PCCO) [19]) and hole-doped ($Bi_2Sr_2CaCu_2O_{8-\delta}$ (Bi2212) [7]) high-T_c cuprates. Pseudogap behavior of the dynamic optical conductivity in the LDA+DMFT+$\Sigma_{\mathbf{k}}$ scheme [16] was also discussed for B12212 [7] and NCCO [8].

Here, we describe LDA+DMFT+$\Sigma_{\mathbf{k}}$ computations of the Fermi surface and spectral functions for the hole-underdoped $La_{1.86}Sr_{0.14}CuO_4$ (LSCO) system supported by high-energy high-resolution bulk-sensitive ARPES [3].

2. COMPUTATIONAL DETAILS

The La_2CuO_4 system has the base-centered orthorhombic crystal structure with space group $Bmab$ with two formula units per cell [20]. The corresponding lattice parameters are $a = 5.3346$, $b = 5.4148$, and $c = 13.1172$ Å. The atomic positions are as follows: La$(0.0, -0.0083, 0.3616)$, Cu(0,0,0), O$(1/4, 1/4, -0.0084)$, and O_2(0.0,0.0404,0.1837).

As a first step of the LDA+DMFT+$\Sigma_{\mathbf{k}}$ method, we performed density functional theory calculations in the local density approximation (LDA) for these crystallographic data. The band structure was obtained with the method of linearized muffin-tin orbitals (LMTO) [21]. It is well known that the Fermi level of these compounds is crossed by the antibonding O2p–Cu3d partially filled orbital of the $x^2 - y^2$ symmetry. Tight-binding parameters for this band were calculated by the N-th order LMTO (NMTO) method [22] as $t = -0.476$, $t' = 0.077$, $t'' = -0.025$, and $t''' = -0.015$ (in eV units). These values agree well with previous studies [23]. The Coulomb interaction value on the effective Cu-3$d(x^2 - y^2)$ orbital was calculated by the constrained LDA approach [24] and was found to be $U = 1.1$ eV. These LDA-obtained parameters are used to set up the corresponding one-band Hubbard model.

The second step is to consider the above-defined Hubbard model using the DMFT self-consistent set of equations [9] supplied by an "external" momentum-dependent self-energy $\Sigma_{\mathbf{k}}$ [11]. The additive form of self-energy (the main approximation of the scheme is to neglect the interference between the Hubbard interaction and pseudogap fluctuations, which allows preserving the conventional DMFT equations) allows defining the LDA+DMFT+$\Sigma_{\mathbf{k}}$ Green's function as

$$G_{\mathbf{k}}(\omega) = \frac{1}{\omega + \mu - \varepsilon(\mathbf{k}) - \Sigma(\omega) - \Sigma_{\mathbf{k}}(\omega)}, \qquad (1)$$

where the bare electron dispersion $\varepsilon(\mathbf{k})$ is defined by the LDA-calculated hopping parameters listed above. To calculate $\Sigma_{\mathbf{k}}$, we used a two-dimensional pseudogap model [1, 15] describing nonlocal correlations induced by (quasi)static short-range collective Heisenberg-like AFM spin fluctuations. Thus we introduce a correlation length dependence of the pseudogap fluctuations into the conventional DMFT loop.

There are two points that make the DMFT+$\Sigma_{\mathbf{k}}$ scheme different from the usual DMFT scheme. First, momentum-dependent $\Sigma_{\mathbf{k}}$ is recalculated at each DMFT iteration ($\Sigma_{\mathbf{k}}(\mu,\omega,[\Sigma(\omega)])$ is in fact a function of the DMFT chemical potential and the DMFT self-energy). Second, the DMFT+$\Sigma_{\mathbf{k}}$ lattice problem is defined at each DMFT iteration as

$$G_{ii}(\omega) = \frac{1}{N}\sum_{\mathbf{k}} \frac{1}{\omega + \mu - \varepsilon(\mathbf{k}) - \Sigma(\omega) - \Sigma_{\mathbf{k}}(\omega)}. \quad (2)$$

After numerical self-consistency is reached, we obtain Green's function (1) with the corresponding $\Sigma(\omega)$ and $\Sigma_{\mathbf{k}}(\omega)$ of the last DMFT iteration. All further computational details can be found, e. g., in Refs. [7, 8, 11].

As an "impurity solver" for DMFT equations, the numerical renormalization group (NRG [25, 26]) was used. The temperature of DMFT(NRG) computations was taken to be 0.011 eV and the electron concentration used was $n = 0.86$.

The self-energy $\Sigma_{\mathbf{k}}(\omega)$ due to pseudogap fluctuations depends on two parameters in general: the pseudogap amplitude Δ and the correlation length ξ [1, 15]. The value of Δ was calculated as in [11],

$$\Delta^2 = U^2 \frac{\langle n_{i\uparrow} n_{i\downarrow}\rangle}{n^2} \langle (n_{i\uparrow} - n_{i\downarrow})^2\rangle, \quad (3)$$

where local densities $n_{i\uparrow}$, $n_{i\downarrow}$ and the double occupancy $\langle n_{i\uparrow} n_{i\downarrow}\rangle$ were calculated within the standard DMFT scheme [9]. The behavior of Δ as a function of hopping integrals and the Coulomb interaction was studied in our previous work [11], while Δ as a function of the occupancy n was investigated in Ref. [7]. For ξ, we believe it is safer to take experimental values. In this work, the value of Δ was calculated to be 0.21 eV and ξ was taken to be $10a$, where a is the lattice constant [27].

3. EXPERIMENTAL DETAILS

The high-energy ARPES measurements were carried out at BL25SU in SPring-8, using incident photons of the energy 500 eV, on single crystal samples. The normal to the cleaved sample surface was set almost parallel to the axis of the analyzer lens and the sample was set at about 45° to the incident light direction. The photoelectrons within polar angles about ±6° to the normal to the sample were simultaneously collected using a GAMMADATASCIENTA SES200 analyzer, thereby covering more than a whole Brillouin zone along the directions of the analyzer slit. The Fermi surface mapping was performed by changing the angle along the direction perpendicular to the analyzer slit. The base pressure was about $4 \cdot 10^{-8}$ Pa. The (001) clean surface was obtained by cleaving the samples in situ in a vacuum at the measuring temperature 20 K. The overall energy resolution was respectively set to 100 and 170 meV for high-resolution measurements and Fermi surface mapping. The angular resolution was ±0.1 (±0.15) for the perpendicular (parallel) direction to the analyzer slit. These values correspond to the momentum resolution $\pm 0.024\pi/a$ ($\pm 0.036\pi/a$) at $h\nu = 500$ eV, where a is twice the Cu–O bond length within the CuO_2 plane. Because the photoelectron mean free path of the order of 12 Å at the kinetic energy of the order of 500 eV is longer than that for conventional ARPES at $h\nu \sim 20$–60 eV, the bulk contribution to the spectral weight is estimated at about 60 %. The position of the Fermi level was calibrated with Pd spectra.

4. RESULTS AND DISCUSSION

For the temperature and the interaction strength, we have to take the finite lifetime effects of quasiparticles into account. Instead of just a dispersion $\varepsilon(\mathbf{k})$, we must then work with the spectral function $A(\omega,\mathbf{k})$ given by

$$A(\omega,\mathbf{k}) = -\frac{1}{\pi}\,\mathrm{Im}\,G(\omega,\mathbf{k}), \quad (4)$$

with the retarded Green's function $G(\omega,\mathbf{k})$ obtained via the LDA+DMFT+$\Sigma_{\mathbf{k}}$ scheme [10, 11, 16]. Of course, there are considerable lifetime effects originating from $\Sigma_{\mathbf{k}}$ corresponding to the interaction with AFM fluctuations (substituted in our approach by a quenched random field).

In Fig. 1*a*, a contour map of spectral function (4) obtained from LDA+DMFT+$\Sigma_{\mathbf{k}}$ for the Cu-$3d(x^2-y^2)$ band is presented. The width of the spectral function is inversely proportional to the lifetime. Around the (π,0) point, we can clearly see the splitting of the spectra by AFM pseudogap fluctuations of the order of 2Δ. The AFM nature of the pseudogap fluctuations also leads to the formation of a "shadow" band, which is much weaker in intensity and becomes the real quasiparticle band in the case of complete folding with a long-range AFM order.

Figure 2 displays experimental energy distribution curves (EDC) in panel (*a*) along the (0,0)–(π,0) direction. Around the (π,0) point, a certain deviation of the $A(\omega,\mathbf{k})$ maxima from the Fermi level (a kind of "turn-back") is observed. We attribute such behavior of $A(\omega,\mathbf{k})$ to pseudogap fluctuations. A similar theoretical behavior shown on panel (*b*) of Fig. 2 is calculated

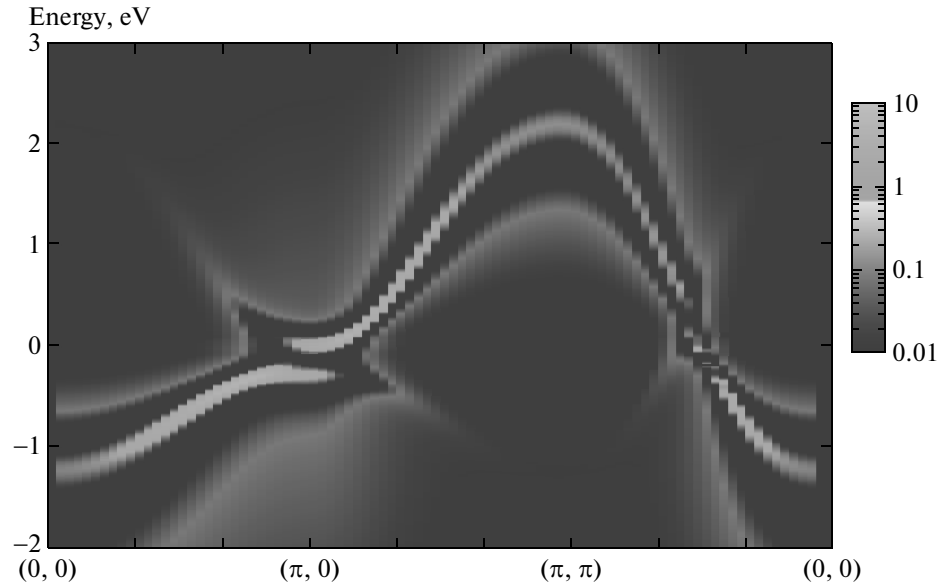

Fig. 1. LCOO Cu-$3d(x^2 - y^2)$ band dispersion along high-symmetry directions of the square Brillouin zone computed with LDA+DMFT+$\Sigma_{\mathbf{k}}$. The Fermi level is zero

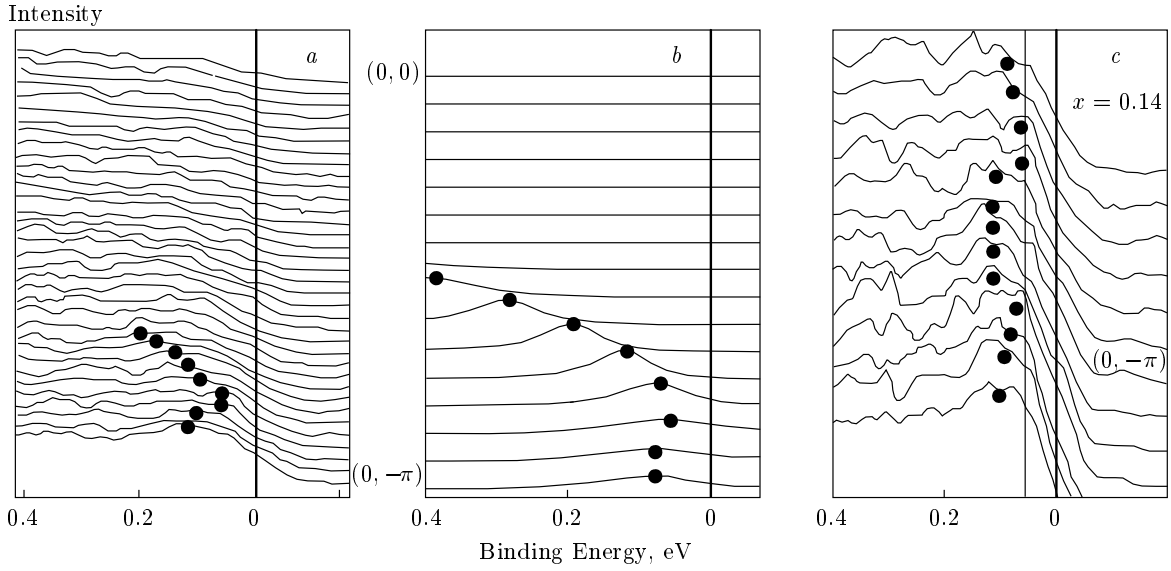

Fig. 2. ARPES EDC curves a and LDA+DMFT+$\Sigma_{\mathbf{k}}$ spectral functions b along the (0,0)–$(\pi, 0)$ high-symmetry direction; ARPES MDC curves c around the $(\pi, 0)$ point for LSCO at $x = 0.14$. On panels a, b, and c, filled circles guide the motion of the $A(\omega, k)$ maxima. The Fermi level is zero

by our LDA+DMFT+$\Sigma_{\mathbf{k}}$ approach (see also Fig. 1)[1)]. The same behavior is also observed (traced by circles) in experimental ARPES momentum distribution curves (MDC) demonstrated on panel c in Fig. 2.

The bulk-sensitive high-energy ARPES data for $La_{1.86}Sr_{0.14}CuO_4$ show a clear "turn-back" structure of the EDC peak as a function of the momentum near $(0,-\pi)$, which were not seen in the previous low-energy ARPES data for $La_{1.85}Sr_{0.15}CuO_4$ [4]. The contour map of the spectral weight in the vicinity of E_F seems to be essentially similar in overall features for this

[1)] Theoretical curves are shifted up by 0.2 eV for better fit with experiment.

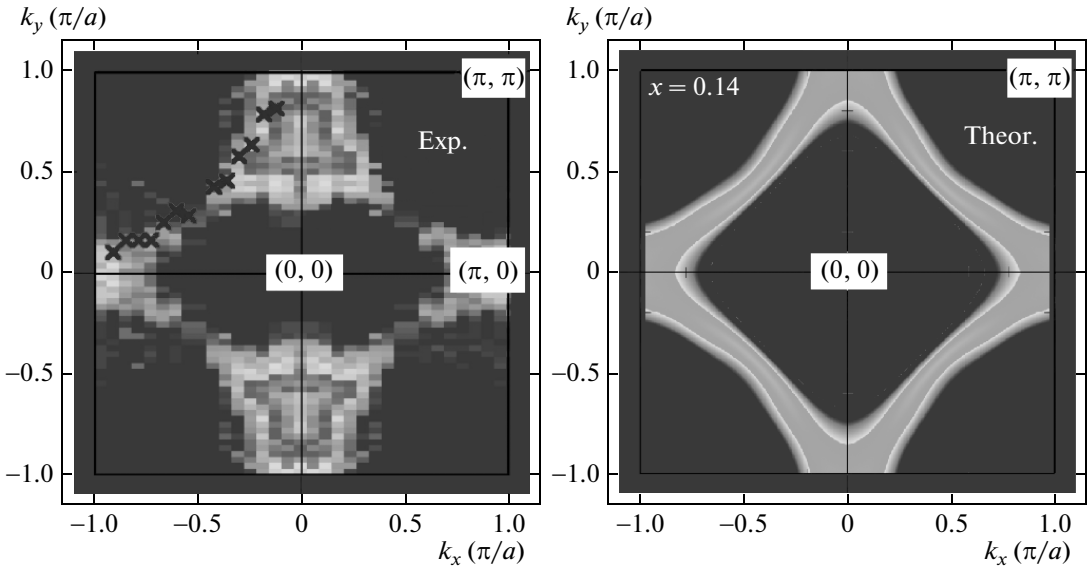

Fig. 3. Fermi surfaces of LSCO at $x = 0.14$ from experiment (left panel) and LDA+DMFT+$\Sigma_{\mathbf{k}}$ computations (right panel). Crosses on the left panel correspond to experimental $\mathbf{k}_F$ values

doping level between the high-energy and low-energy ARPES studies.

Experimental and theoretical Fermi surface maps are shown in Fig. 3. Both pictures reveal strong scattering around the (π,0) point, which we associate with scattering in the vicinity of the so-called "hot spots" (crossing points of the Fermi surface and the AFM umklapp surfaces) that are close to (π,0) [7, 8]. Such a strong scattering comes from scattering processes with momentum transfer of the order of $\mathbf{Q}=(\pi,\pi)$ [1, 15], corresponding to AFM pseudogap fluctuations. Along the nodal directions, we observe typical Fermi arcs. They are quite well seen in the theoretical data, while in the experiment, we have just narrow traces of them.

5. CONCLUSION

Our LDA+DMFT+$\Sigma_{\mathbf{k}}$ hybrid approach was shown to be an effective numerical tool to describe the short-range ordered state in quasi-two-dimensional systems [7, 8, 19]. Material-specific model parameters such as hopping integrals (which define the bare electron band dispersion of the effective Cu3$d(x^2-y^2)$ orbital) were calculated via an LDA-based NMTO method [22]. The Coulomb interaction parameter U was obtained from the constrained LDA method. The pseudogap amplitude Δ was computed using the LDA+DMFT scheme [8, 11]. Supplementing the conventional DMFT self-energy by $\Sigma_{\mathbf{k}}(\omega)$ describes nonlocal dynamic correlations due to short-range collective Heisenberg-like AFM spin fluctuations.

In this work, we performed LDA+DMFT+$\Sigma_{\mathbf{k}}$ calculations for the hole-doped $La_{1.86}Sr_{0.14}CuO_4$ compound in the pseudogap regime. Because of fluctuations of the AFM short-range order, we clearly observe formation of the so-called "shadow bands" as partially folded bare dispersion. A pseudogap is formed around the (π,0) point, which is qualitatively the same as in Bi2212 [7], NCCO [8], and PCCO [19]. The Fermi surface of LSCO is similar to that obtained for Bi2212 [7]. Namely, the "hot spots" are not well resolved because the crossing point of the bare Fermi surface and the AFM umklapp surface are very close to the Brillouin zone border. This is essentially due to the shape and size of the LDA Fermi surface. In this respect, the situation here is different from that for NCCO [8] and PCCO [19], where "hot spots" are clearly seen. To support these theoretical results, we here present new high-energy, high-resolution ARPES data for LSCO. Typical pseudogap-like effects of the Fermi surface destruction were observed in both theory and experiment. The same is true for spectral functions. The overall semi-quantitative agreement between theory and experiment basically supports our general picture of the pseudogap state as being due to strong scattering of carriers by short-range AFM order fluctuations.

We thank Thomas Pruschke for providing us with the NRG code. This work is supported by the RFBR (grants №№ 08-02-00021 and 08-02-91200) and the RAS programs "Quantum physics of condensed matter" and "Strongly correlated electrons solids". I. N. is supported by President Grant MK-614.2009.2(IN) and the Russian Science Support Foundation. A. S. and S. S. acknowledge JSPS for the financial support of the joint Japan–Russia research in 2008–09. They also acknowledge MEXT, Japan for a Grant-in-Aid for scientific research (18104007, 15GS0123, 18684015).

REFERENCES

1. T. Timusk and B. Statt, Rep. Progr. Phys. **62**, 61 (1999); M. V. Sadovskii, Usp. Fiz. Nauk **171**, 539 (2001); M. V. Sadovskii, in *Strings, Branes, Lattices, Networks, Pseudogaps, and Dust*, Scientific World, Moscow (2007), p. 357.
2. A. Damascelli, Z. Hussain, and Zhi-Xun Shen, Rev. Mod. Phys. **75**, 473 (2003).
3. M. Tsunekawa, A. Sekiyama, S. Kasai et al., New J. Phys. **10**, 073005 (2008).
4. T. Yoshida, X. J. Zhou, K. Tanaka et al., Phys. Rev. B **74**, 224510 (2006).
5. V. J. Emery and S. A. Kivelson, Nature **374**, 434 (2002).
6. A. A. Kordyuk, S. V. Borisenko, V. B. Zabolotnyy et al., Phys. Rev. B **79**, 020504(R) (2009).
7. E. Z. Kuchinskii, I. A. Nekrasov, Z. I. Pchelkina, and M. V. Sadovskii, Zh. Eksp. Teor. Fiz. **131**, 908 (2007); I. A. Nekrasov, E. Z. Kuchinskii, Z. V. Pchelkina, and M. V. Sadovskii, Physica C **460–462**, 997 (2007).
8. E. E. Kokorina, E. Z. Kuchinskii, I. A. Nekrasov et al., Zh. Eksp. Teor. Fiz. **134**, 968 (2008); I. A. Nekrasov et al., J. Phys. Chem. Sol. **69**, 3269 (2008).
9. A. Georges, G. Kotliar, W. Krauth, and M. J. Rozenberg, Rev. Mod. Phys. **68**, 13 (1996).
10. E. Z. Kuchinskii, I. A. Nekrasov, and M. V. Sadovskii, Pis'ma v ZhETF **82**, 217 (2005).
11. M. V. Sadovskii, I. A. Nekrasov, E. Z. Kuchinskii, Th. Prushke, and V. I. Anisimov, Phys. Rev. B **72**, 155105 (2005).
12. E. Z. Kuchinskii, I. A. Nekrasov, and M. V. Sadovskii, Fizika Nizkikh Temperatur **32**, 528 (2006).
13. E. Z. Kuchinskii, I. A. Nekrasov, and M. V. Sadovskii, Phys. Rev. B **80**, 115124 (2009).
14. E. Z. Kuchinskii, I. A. Nekrasov, and M. V. Sadovskii, Zh. Eksp. Teor. Fiz. **133**, 670 (2008).
15. J. Schmalian, D. Pines, and B. Stojkovic, Phys. Rev. B **60**, 667 (1999); E. Z. Kuchinskii and M. V. Sadovskii, Zh. Eksp. Teor. Fiz. **115**, 1765 (1999).
16. E. Z. Kuchinskii, I. A. Nekrasov, and M. V. Sadovskii, Phys. Rev. B **75**, 115102 (2007).
17. R. O. Jones and O. Gunnarsson, Rev. Mod. Phys. **61**, 689 (1989).
18. K. Held, I. A. Nekrasov, G. Keller et al., Psi-k Newsletter **56**, 65 (2003); K. Held, Adv. Phys. **56**, 829 (2007).
19. I. A. Nekrasov, N. S. Pavlov, E. Z. Kuchinskii et al., Phys. Rev. B **80**, 115124(R) (2009).
20. M. Braden, P. Schweiss, G. Heger et al., Physica C **223**, 396 (1994).
21. O. K. Andersen, Phys. Rev. B **12**, 3060 (1975); O. K. Andersen and O. Jepsen, Phys. Rev. Lett. **53**, 2571 (1984).
22. O. K. Andersen and T. Saha-Dasgupta, Phys. Rev. B **62**, R16219 (2000); O. K. Andersen et al., Psi-k Newsletter **45**, 86 (2001); O. K. Andersen, T. Saha-Dasgupta, and S. Ezhov, Bull. Mater. Sci. **26**, 19 (2003).
23. M. M. Korshunov, V. A. Gavrichkov, S. G. Ovchinnikov et al., Zh. Eksp. Teor. Fiz. **126**, 642 (2004).
24. O. Gunnarsson, O. K. Andersen, O. Jepsen, and J. Zaanen, Phys. Rev. B **39**, 1708 (1989).
25. K. G. Wilson, Rev. Mod. Phys. **47**, 773 (1975); H. R. Krishna-murthy, J. W. Wilkins, and K. G. Wilson, Phys. Rev. B **21**, 1003, 1044 (1980).
26. R. Bulla, A. C. Hewson, and Th. Pruschke, J. Phys.: Condens. Matter **10**, 8365 (1998).
27. M. Hcker, Young-June Kim, G. D. Gu, J. M. Tranquada, B. D. Gaulin, and J. W. Lynn, Phys. Rev. B **71**, 094510 (2005).